Al-Mustansiriyah Journal of Science
ISSN: 1814-635X (print), ISSN:2521-3520 (online) Volume 34, Issue 4, 2023 DOI: https://doi.org/10.23851/mjs.v34i4.1401

Research Article **Open Access**

Optical and Electrical Properties of Nano Magnesium Oxide Doped with Polyvinylpyrrolidone (PVP)Thin Films

Zainb D. Abd Ali[1*], Ahamed A. Ahamed[1], Osama Abdul Azeez Dakhil[1], Ali Albeer[2]

[1] Department of Physics, College of Science, Mustansiriyah University, 10052 Baghdad, IRAQ.
[2] Biometry and epidemiology (IBE), Institute of medical information processing, Ludwig Maximilian University of Munich (LMU), Germany.

*Correspondent contact: zainabdakheel@uomustansiriyah.edu.iq

Article Info

Received
16/05/2023

Revised
27/05/2023

Accepted
11/06/2023

Published
30/12/2023

ABSTRACT

A thin film of polyvinylpyrrolidone (PVP) polymer doped with different weight ratios of magnesium oxide nanoparticles produced by using the low-temperature hydrothermal method was prepared, and the morphology of the doped thin film was verified using a scanning electron microscope and an atomic force microscope. The X-ray diffraction pattern showed that magnesium oxide has a multicubic crystal structure with a diffraction peak of high density associated with the level (200) (at the diffraction angle of 42.69°) and a crystal drop size of 25 nm. Measurements of the Fourier A transformation of the infrared spectrum of a polyvinylpyrrolidone polymer doped with metal oxides was carried out. It showed a clear difference from the pure polymer, where a (Mg-O-Mg) bond appeared at a wavelength of 450 cm^{-1} to confirm the effect of MgO addition on the chemical bonding of polyvinylpyrrolidone. Optical properties, including absorbance, maximum wavelength, and energy gap, have been studied. Determined by ultraviolet examination. The band gap decreased when MgO was doped with PVP films, and the Hall coefficient effect was used to calculate the electrical properties, including the conductivity, kinetics of charge carriers, and their type. The highest conductivity was (0.1×10^{-2} Sm), and the tainted membrane was of the n type, where it can be used in optical applications.

KEYWORDS: PVP polymer, magnesium oxide nanoparticle, hydrothermal synthesis, electric conductivity, composite thin film, conductive polymer.

الخلاصة

تم تحضير أغشية من بوليمر بولي فاينيل بيرليدون مشوبة بنسب وزنية مختلفة من جسيمات اوكسيد المغنيسيوم النانوي التي انتجت باستخدام الطريقة الحرارية المائية ذات الدرجات الحرارية المنخفضة وتم التحقق من مورفولوجية الاغشية المشوبة باستخدام المجهر الالكتروني الماسح و مجهر القوة الذرية .اظهر نمط حيود الاشعة السينية ان اوكسيد المغنيسيوم له تركيب بلوري متعدد مكعب مع قمة حيود ذات كثافة عالية مرتبطة بالمستوى (٢٠٠) (عند زاوية الحيود=٤٢,٦٩° (مع حجم بلوري قطرة ٢٥ نانومتر .أجريت قياسات تحويل فورييه للطيف بالأشعة تحت الحمراء لبوليمر بولي فاينيل بيرليدون المشوب بأكاسيد المعدن النانوية , حيث اظهر اختلاف واضح عن البوليمر النقي حيث ظهرت رابطة Mg-O-Mg) (عند الطول الموجي) ٤٥٠ سم. تم دراسة الخصائص البصرية بما في ذلك الامتصاصية ، الطول الموجي الأقصى ، وفجوة الطاقة. يحددها فحص الأشعة فوق البنفسجية. لتأكيد تأثير إضافة MgO على الترابط الكيميائي لأفلام بولي فاينيل بيرليدون تم استخدام تأثير معامل هول لحساب الخصائص الكهربائية بما في ذلك التوصيلية حركية ناقلات الشحنة ونوعها. أعلى توصيلية كانت ($0.1*10^{-2}$سيمنز) والغشاء المشوب كان من نوع (n type) حيث يمكن استخدامه في التطبيقات البصرية.

INTRODUCTION

Petrochemical-based conductive polymers CPs have been attracting much attention CPs have benefits such as low density, chemical variety, flexibility, adaptable conductivity, easily controllable form, and morphogenesis [1]. Consequently, they might be used in large-area optoelectronic devices [2], absorption of microwaves materials, different kinds of sensors, storage of energy engineering, anticorrosive coating, physiological field.

The conductive polymer is a very brittle organic substance that exhibits electrical conductivity as a result of its distinct structure. Numerous methods, such as electrochemical, chemical, hydrogel composite, spin coating, and electrospinning

procedures, can be used to produce conductive polymers. Conductive polymers often possess the -conjugated system with alternate single and double bonds, which gives rise to their intrinsic electrical/electronic, electrochemical, and optical capabilities so transport electricity without the use of metallic additions, in contrast to conventional conductive composites formed by combining insulating polymers and metals [2].

Conductive polymer composites (CPCs) are artificial materials that have just two components: conducting charges and an insulating matrix. The "reinforcement" is often created from, While the matrix is often a polymer with electrical insulating properties, certain electrically conducting charges are introduced in various combinations [3]. The following are the four main types of conductive charges used in CPCs:

1. Ionic compounds such as NaCl, KOH, NH4F, CaCl2, ...
2. Metallic as aluminum, nickel, copper, silver, etc.
3. Carbon derivatives such as (graphene, fullerene derivatives, carbon nanotubes, and graphite)
4. inherent conductive polymer like Poly (3,4-ethylene dioxythiophene) PEDOT [4].

The conductivity is enhanced by an increase in dopant concentration. Due to the conductive polymers' organized, dense structure, the dopant ions slowly diffuse into them in the meantime. The conductivity grew progressively saturated after a lengthy doping period, perhaps even several hours. Additionally, the process of doping and dedoping can be reversed Electrical characteristics When the concentration of conductive charges relative to the polymer matrix composition rises in conductive polymer composites (CPCs), the electrical conductivity likewise rises [5].

The dopants can be divided into large polymeric species and tiny cations/anions, increasing their conductivity by five or more orders of magnitude in the semiconductor regime [6][7]. Due to their tight bonds to the polymer chain, large dopants are difficult to remove. Additionally, they affect the CPs' density, surface topography, and physical characteristics. Small dopants, in contrast, quickly and easily dope the CPs and quickly dedupe, resulting in low stability. The concentration of the dopant and the doping time significantly impact the conductivity of CPs, which increases as the doping level increases. The conductivity is improved as the dopant concentration rises. Due to the conductive polymers' dense, organized structure, the dopant ions diffuse into them over time. The conductivity grew progressively saturated after a lengthy doping period, perhaps even several hours.

MATERIALS AND METHODS

For preparation the magnesium oxide nanoparticles, liquids of magnesium nitride as Mg $(NO_3)2.6H_2O$ and HMT ($C_6H_{12}N_4$) were dissolved in 80 ml of water while being stirred. [all material purchased from Sigma-Ald]. The concentration (weight in grams) of Mg nitrate and (HMT) is instructed by the molarity (M) of the solution (Equation 1 [9]), which is 5%, by [8].

$$M\% = \frac{W}{M.W} \times \frac{1000}{V} \quad (1)$$

The chemical reaction to produced MgO NPs are [10][11]:

$$(CH_2)6N_4 + 6H_2O \rightarrow 6HCHO + 4NH_3 \quad (2)$$

$$NH_3 + H_2O \rightarrow NH^{4+} + OH^- \quad (3)$$

$$Mg^{+2} + 4NH_3 \rightarrow Mg(NH_3)\,4^+ \quad (4)$$

Mg+ is drawn to the OH surrounding the nanocrystal, forming a virtual capping layer that prevents the nanocrystal from developing [12][13].

$$Mg^{2++}\,2OH \longleftrightarrow Mg(OH)_2 \quad (5)$$

$$Mg(OH)2 + 2OH^- \longleftrightarrow [Mg(OH)_4]^{2-} \quad (6)$$

$$[Mg(OH)4]^{2-} \longleftrightarrow MgO_2{}^{2-} + 2H_2O \quad (7)$$

$$MgO2^{2-} + H_2O \longleftrightarrow MgO + 2OH^- \quad (8)$$

Pure crystals of MgO were produced. One or more of the experimental growth parameters that have a substantial impact on the morphology and aspect ratio are the initial solution pH, precursor concentration, and growth temperature [14][15].

1 gm of PVP solvent in 50 ml of water (2%wt of PVP) at 80 °C for 60 min, concentrations of MgO NPs added to the solution with (0.01, 0.02, 0.03, 0.04. 05, .06, 0.07, 0.08. 0.09, and 0.1) gm, the thin film prepared by the casting method After cooling the solution polymer, the solutions must be cast on a glass Petri dish to form a thin film. It takes about (2 days) to form a thin film with 1µm of thickness

ISSN: 1814-635X (print), ISSN:2521-3520 (online) Volume 34, Issue 4, 2023 DOI: https://doi.org/10.23851/mjs.v34i4.1401

measured by (COATING THICKNESS METER CM8829S) as shown in Figure 1.

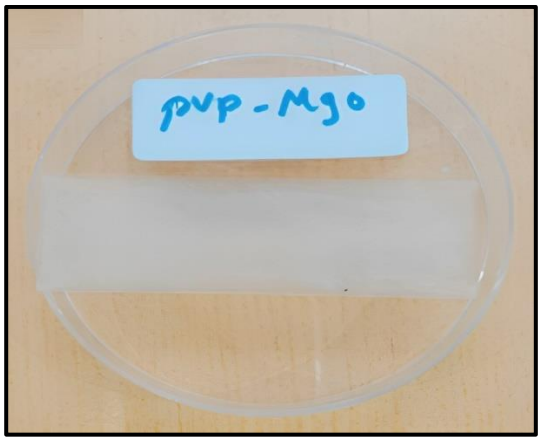

Figure 1. PVP-MgO thin film composite.

RESULTS AND DISCUSSION

Morphology and Structural

Figure 2 shows the MgO nano powder produced by hydrothermal method that was analyzed using an X-ray diffraction instrument. The results of the MgO NPs data showed the presence of diffraction peaks at the angles 29.2, 31.8, 42.8, 47.8, 62, 74, and 78.4, which correspond to the Miller indices (111), (200), (220), (311), and (222) [1-3]. These planes pertain to the creation of crystalline cubic structure of MgO nanoparticles [16]. The XRD of the Mgo pattern shows no additional phases. while diffraction peaks located at the 2θ value of 29.2, 31.8, ~49, and ~64 are indicated Mg(OH)2 compound [17][18] Where these peakS disappear when calcined degree over 500 [19].

By applying the diffraction intensity of the (200) peak and Scherrer's equation, the crystalline size of the samples was calculated. According to the growth conditions, the particles' crystalline size (D) ranged from 25 to 91 nm. The data of MgO NPs XRD spectrum analysis is illustrated in Table 1. The XRD Pattern spectra results of MgO NPs matched with [20][21]. The diffraction peaks are in good agreement with the standard pattern of face-centered cubic (FCC) MgO (JCPDS file no. 77-2364) with a space group of Fm-3m. MgO nanostructures [22].

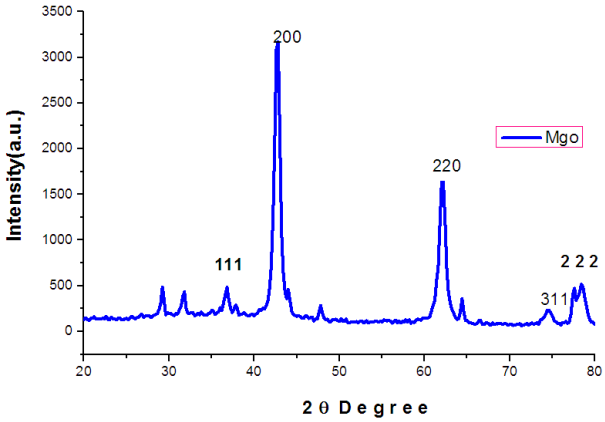

Figure 2. XRD pattern of MgO NPs.

Table 1. The structural parameters of MgO NPs.

2Θ (deg)	FWHM (deg)	Crystal Size (nm)	Intensity (a.u)	Miller index (hkl)
36.7731	0.6845	56.82008	176	111
42.6993	0.8085	25.41533	2007	200
62.0679	0.8529	57.72235	1074	220
74.5119	0.9496	37.0485	102	311
77.4192	0.4222	43.51832	249	222

The FTIR spectrum was determined for the pure PVP and composite thin film of PVP-MgO nanostructure, which is displayed in Figure 3.

Figure 3-a shows the distinct feature bands of PVP pure, which are: [O-H] stretching corresponding 3434 cm^{-1}, a symmetric stretching for [C-H] at 2955 cm^{-1} ,a t 1661 cm^{-1} of wave number there is (C=O) stretching vibration In the FTIR spectrum, the (C=O) groups of pure PVP exhibit a strong peak at 1661.4 cm^{-1}, which is typical of the amide (C=O) bond seen in PVP while CH2 bending vibration sit at 1424 cm^{-1} and the two peaks from 1291 to1018 have been attributed to C−N stretching (23.24).

Figure 3b represents two IR spectra, the blueline belonging to PVP and the red line to PVP doped with 0.2%wt MgO NPs. From the Figure, we can notice that there is an increase in intensity and shifting to the right when MgO NPs added to PVP ma ix in PVP chemicals bands which mean there is an interaction between MgO NP and PVP.

Increased intensity refers to the existence of new chemical bonds at these wave numbers while shifting to the right evidence that the bonds have relation with PVP chemical bonds. When MgO NP reacts with PVP, its peaks in the range of 700–450

cm^{-1} are attributed to various Mg-O-Mg vibration modes of metal oxide and at 1660 cm^{-1} with carbonyl group [19][25]. The broad band amide 3500-3330 cm-1and 1450-1400 cm-1 are attributed to stretching and bending vibration of -OH, respectively, which indicate that the bare MgO surface easily absorbs water when exposed to the environment. A peak at 1654 cm^{-1} in PVP-modified MgO is attributed to the C-O stretching mode of vibration in PVP, providing conclusive proof of the interaction between MgO and PVP. The additional active groups in PVP and MgO are likewise present in the 1200–1300 cm1 range [26].

Several groups have investigated the characteristics of the envelopment of NPs by PVP, almost entirely using vibrational spectroscopy. The prevailing conclusion is that the pyrrolidone ring bonds to the NP by reacting with the carbonyl to create an alkoxide. This appears to be entirely predicated on the small change in the carbonyl stretch's IR peak at 1660 cm -1 after reacting with MgO NPs. Nonetheless, a spectral shift of 1654 cm-1 [19].

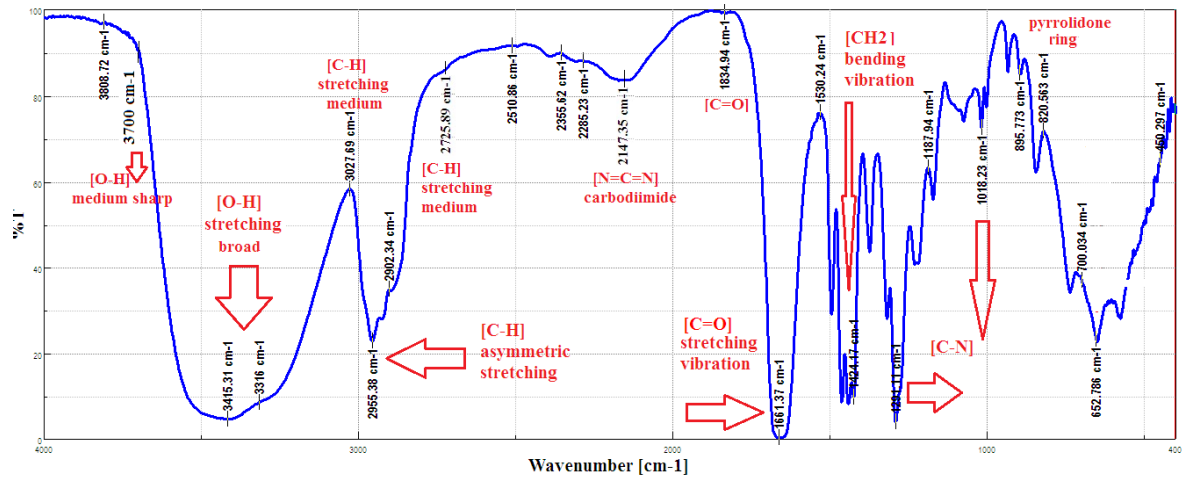

(a)

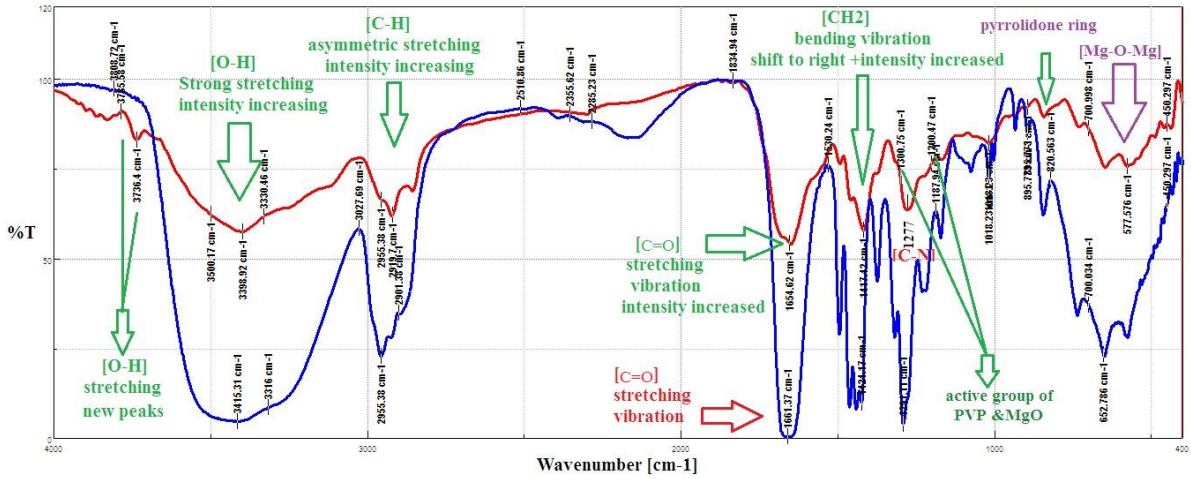

(b)

Figure 3. (a) FTIR for PVP pure, (b) FTIR for overlapping between PVP pure (blue line) & PVP doped with MgO with 0.2 wt% (red line).

MgO NPs features are depicted Figure 4 with a high-density image of scanning electron microscopic (SEM), synthesized via a hydrothermal approach, Figure 4-a demonstrates magnification of MgO NPs 1µm, while a Histogram of The FE-SEM represented in images (c,d), according to calculation of Image J software program has been selected 100 particles as a minimum indicates that the particles have a an average diameter of 29.23 nm. MgO NPs particles ranged in size from 15.6 nm at their smallest to 75 nm at their largest. While PVP-Composite MgO NPs have an average diameter 30 nm. MgO particles ranged in size from 15 nm at their smallest to 50. nm at their largest.

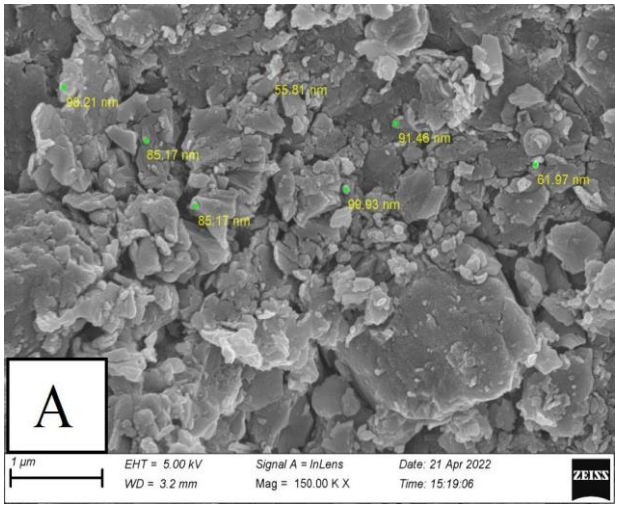

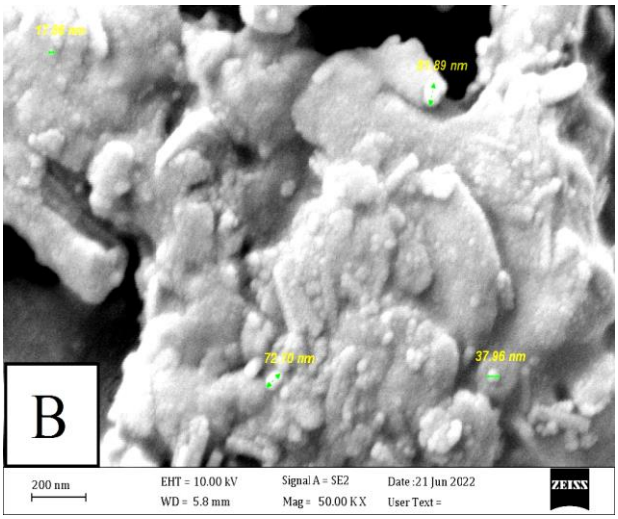

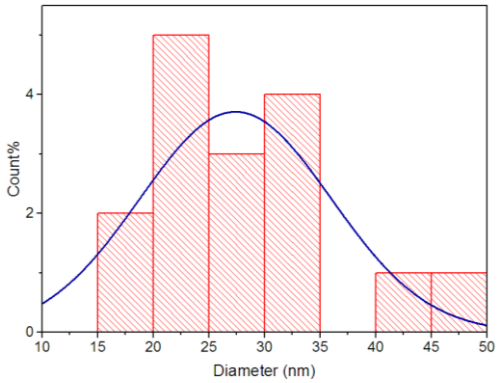

Figure 4. FESEM images of MgO nanoparticles (a) FESEM images of MgO nanoparticles with 1µm scale and (b) PVP-MgO NPs composite thin film 200 nm scale respectively exhibit particles size (c) Histogram of the FE-SEM of MgO nanoparticles with size distributions.

The surface topography and morphology of a PVP-MgO NPs composite thin film were analyzed by atomic force microscopy (AFM) for the sample with nano- and micron-scale dimensions shown in Figure 5 in two dimensions and three dimensions, respectively.

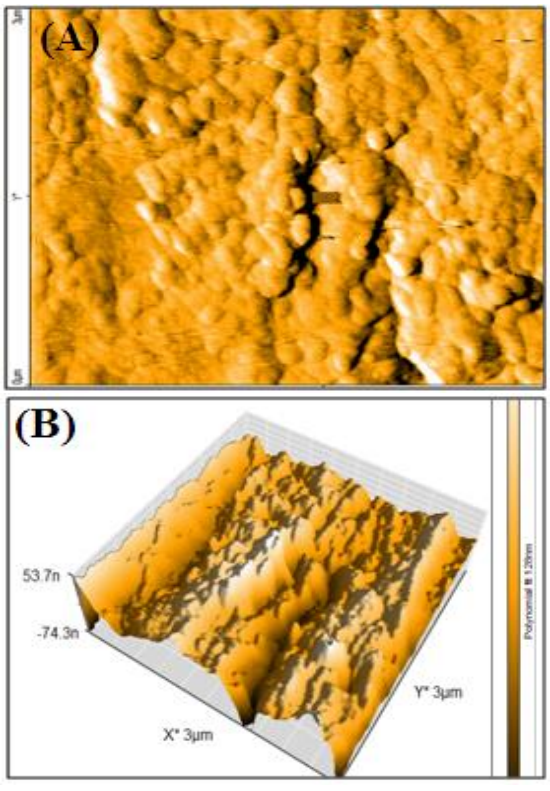

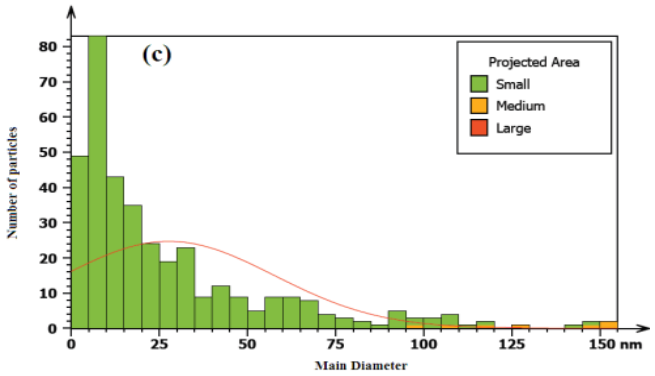

Figure 5. Section line analysis, (A) Topography 2D, (B) Morphology 3D AFM images, and (C) Particle size distribution of PVP-MgO composite thin film.

It is known that the morphology of the film greatly depends on the formation of nanoporous structures within a thin composite film. The image shown in Figure 5 indicates that after impregnation of MgO nanoparticles into the composite thin film, the surface becomes much more homogeneous, and the dimensions of most of the particles were smaller than (1.0 μm), which could be due to aggregation of the MgO nanoparticles, which is a very common phenomenon in nanomaterials synthesis. Mean root square height and mean diameter are significant parameters associated with surface roughness with values at the nanoscale, as seen in figure 4-c which is consistent with the findings of (SEM IMAGE), which depict particles with nano-scale sizes. This confirms that the casting process is a successful method for the synthesis of a thin film without affecting the nano-size of the MgO particles that are inserted in the PVP matrix.

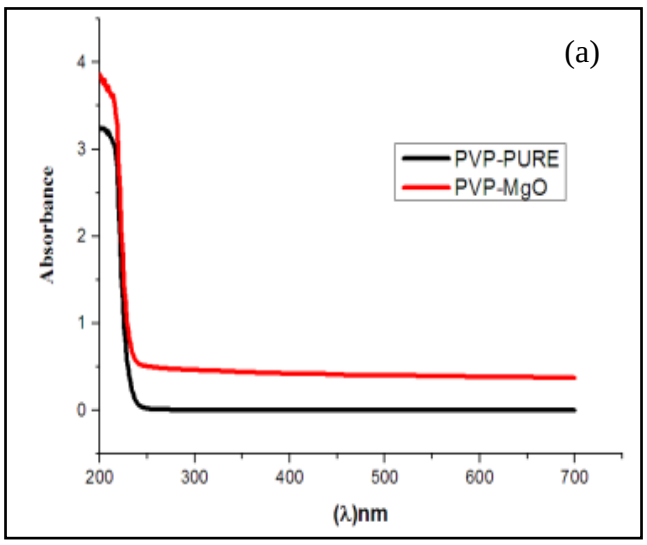

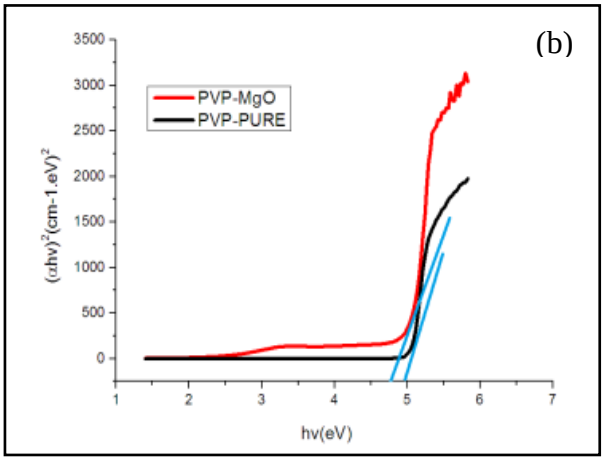

Figure 6. (a) UV-Spectra analysis (Absorption spectra versus the wavelength) for PVP Pure thin film (black line) and PVP-MgO Composite thin film (red line) depicted their Absorption versus of their Wave length. (b) Energy band gap of PVP Pure thin film (black line) and Energy band gap of PVP-MgO Composite thin (red line)

Figure 6 the curve depicted the relation between (hν) and $(\alpha h\nu)^2$, where the band gap energy of the thin film is represented by the intercept between the lowest point in the curve and the x-axis, which is (4.9 eV) for PVP pure, and the result coincided with Pan, Mingming, et al. (2020) [27] and Vani, G. Naga Sudha *et al.* 2013 [28].

Figure 6-b shows that the band gap energy for a thin film of PVP doped with wt%0.2 MgO NPs is 4.7 eV smaller than that of PVP pure. This finding is in agreement with Mohammed, M. I., et al. (2022) [22]; MgO NPs have a large band gap because their optical band gap is 4.5 eV as opposed to 7.8 eV for bulk MgO's regular structure. [29][30].

Hall Effect's advantage is due to its competence to precisely measure the properties of a specimen of any arbitrary and irregular shape. In practically two dimensions, the sample is thin and solid (no holes), and "The Van der Pauw method" [31] has four electrodes with the placement of 1cm around the perimeter of the specimen, and employs a linear four-point probe. [32]

Then the measurements are made. The properties of the matter that are calculable are the resistivity and conductivity of the material, the doping type (i.e., whether it is a P-type or N-type material), and the mobility of the majority of the carriers shown in Table 2. The Equation (9) [33][34] can be performed to calculate the films' resistance (ρ):

$$\rho = R \cdot W \cdot t / L \qquad (9)$$

W is the electrode's width, L is the distance between the electrodes, and t is the thin film's

thickness, where R is the resistance. The conductivity (σ) of the film, based on the relationship [1,35], could be specified in Equation (10), as follows:

$$\sigma = 1/\rho \qquad (10)$$

From Figure 7, the conductivity of the thin film PVP-MgO NPs composite is calculated and plotted as a function of the concentration of MgO NPs doping with different concentrations in the following order: (0.01, 02,03, 04, 05, 06, .07.08.09,0.1) gm, the maximum conductivity is (1.091×10^{-4}) Sm corresponding to a concentration of 0.1 gm, the conductivity is increased with concentrations. The conductivity, average hall coefficient, charge type, and mobility for MgO NPs at different concentrations are listed in Table 2. The thin film is N-type doping. The conductivity of pure PVA ranges from 10^{-9} to 10^{-11}. The doping process with MgO NPs increases electrical conductivity by increasing the concentrations of MgO NPs, resulting in a semiconductor made of PVA–MgO NPs composite thin film. The highest value of conductivity was obtained when it was concentrated on MgO NPs, which is 0.1 gm.

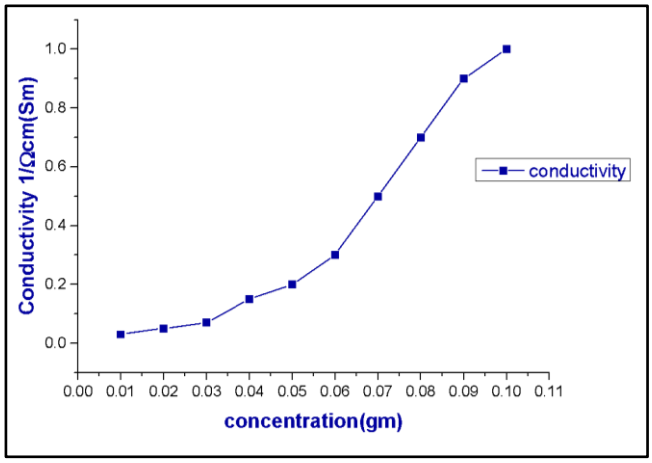

Figure 7. Relationship between conductivity and concentration of PVP- MgO NPs thin film.

Table 2. Measurements of hall effect of PVP-NiO thin films.

Concentration (gm)	Conductivity 1/Ω.cm (Sm)	Avarage Hall Coefficient (m2/c)	Mobility (cm2 /vs)
0.01	$0.0\ 3343\times10^{-5}$	$-1.91545\times10^{+6}$	$1.5841\times10^{+2}$
0.02	$0.\ 05296\times10^{-5}$	$-1.97144\times10^{+6}$	$1.8567\times10^{+2}$
0.03	$0.\ 07264\times10^{-5}$	$-2.01248\times10^{+6}$	$1.9863\times10^{+2}$
0.04	$0.\ 1542\times10^{-3}$	$-2.10852\times10^{+5}$	$2.0847\times10^{+2}$
0.05	$0.\ 2121\times10^{-3}$	$-2.21439\times10^{+5}$	$2.1325\times10^{+2}$
0.06	$0.\ 3086\times10^{-3}$	$-2.3131\times10^{+5}$	$2.1983\times10^{+2}$
0.07	$0.\ 5058\times10^{-3}$	$-2.4138\times10^{+5}$	$2.2438\times10^{+2}$
0.08	$0.\ 7027\times10^{-3}$	$-2.5166\times10^{+5}$	$2.2947\times10^{+2}$
0.09	$0.\ 938\times10^{-3}$	$-2.6089\times10^{+5}$	$2.3574\times10^{+2}$
0.1	$0.\ 1091\times10^{-2}$	$-2.7627\times10^{+4}$	$2.443\times10^{+2}$

CONCLUSIONS

Magnesium oxide nanoparticles were synthesized using the hydrothermal method, and the results of the SEM examination gave the smallest size of the nanoparticles at 25.1 nm. The XRD examination was used to confirm the crystallinity of the nanomaterial that was synthesized. The results showed the presence of sharp peaks in the diagram with the calculation of Miller indices. The cubic form structure of the nanoparticles of magnesium oxide nanoparticles, the particles' crystalline size (D) was calculated to range from 25 to 91 nm. A composite thin film of PVP-MgO NPs was prepared. PVP and MgO NPs active groups are determined by FTIR for composite thin film. The surface topography of the thin film was studied using AFM. The results showed homogeneity of the particles on the surface of the membrane, with the appearance of surface roughness due to the presence of nanostructures in the thin film composition. The optical properties of the doped thin film were studied, and the results showed an increase in absorbance doped films comparable with pure, while the energy gap decreased for the doped film compared to the pure film by 0.2 eV. The conductivity was calculated for thin film doped with different concentrations using the Hall effect, and it was found that the best conductivity was obtained when the concentration of 0.2 wt% MgONPs was 0.1091×10^{-2} and the doped thin film was an N-type charge. As a result, a composite thin film of PVA-MgONPs can be utilized as a semiconductor in photo applications.

ACKNOWLEDGMENTS

The authors would like to thank the Department of Physics, College of Sciences, Mustansiriyah University, Baghdad, Iraq.

Disclosure and conflict of interest: The authors declare that they have no conflicts of interest.

REFERENCES

[1] Addition on the electrical conductivity of polyvinyl alcohol films." American Journal of Engineering Research 6.1 (2017): 337-343.

[2] Koncar, V. "Smart textiles for monitoring and measurement applications." Smart Textiles for In Situ Monitoring of Composites (2019): 1-151. https://doi.org/10.1016/B978-0-08-102308-2.00001-2

[3] Jlassi, Khouloud, Mohamed M. Chehimi, and Sabu Thomas. Clay-polymer nanocomposites. Elsevier, 2017.

[4] Pang, Huan, et al. "Conductive polymer composites with segregated structures." Progress in Polymer Science 39.11 (2014): 1908-1933. https://doi.org/10.1016/j.progpolymsci.2014.07.007

[5] Abdelaziz, M., and Magdy M. Ghannam. "Influence of titanium chloride addition on the optical and dielectric properties of PVA films." Physica B: Condensed Matter 405.3 (2010): 958-964. https://doi.org/10.1016/j.physb.2009.10.030

[6] Le, Thanh-Hai, Yukyung Kim, and Hyeonseok Yoon. "Electrical and electrochemical properties of conducting polymers." Polymers 9.4 (2017): 150. https://doi.org/10.3390/polym9040150

[7] Goel, Mahima, et al. "Principles of structural design of conjugated polymers showing excellent charge transport toward thermoelectrics and bioelectronics applications." Macromolecular Rapid Communications 40.10 (2019): 1800915. https://doi.org/10.1002/marc.201800915

[8] Hornak, Jaroslav. "Synthesis, properties, and selected technical applications of magnesium oxide nanoparticles: a review." International Journal of Molecular Sciences 22.23 (2021): 12752. https://doi.org/10.3390/ijms222312752

[9] Krishnamurthy, Vijay M., et al. "Dependence of effective molarity on linker length for an intramolecular protein− ligand system." Journal of the American Chemical Society 129.5 (2007): 1312-1320. https://doi.org/10.1021/ja066780e

[10] Krajian, H., et al. "Hydrothermal growth method for the deposition of ZnO films: Structural, chemical and optical studies." Microelectronics Reliability 125 (2021): 114352. https://doi.org/10.1016/j.microrel.2021.114352

[11] Hornak, Jaroslav. "Synthesis, properties, and selected technical applications of magnesium oxide nanoparticles: review." International Journal of Molecular Sciences 22.23 (2021): 12752. https://doi.org/10.3390/ijms222312752

[12] Ding, Yi, et al. "Nanoscale magnesium hydroxide and magnesium oxide powders: control over size, shape, and structure via hydrothermal synthesis." Chemistry of materials 13.2 (2001): 435-440. https://doi.org/10.1021/cm000607e

[13] Devaraja, P. B., et al. "Synthesis, structural and luminescence studies of magnesium oxide nanopowder." Spectrochimica Acta Part A: Molecular and Biomolecular Spectroscopy 118 (2014): 847-851. https://doi.org/10.1016/j.saa.2013.08.050

[14] Duong, Thi Hai Yen, et al. "Synthesis of magnesium oxide nanoplates and their application in nitrogen dioxide and sulfur dioxide adsorption." Journal of Chemistry 2019 (2019). https://doi.org/10.1155/2019/4376429

[15] Devaraja, P. B., et al. "Synthesis, structural and luminescence studies of magnesium oxide nanopowder." Spectrochimica Acta Part A: Molecular

[16] Aboud, N. A., B. E. Jasim, and A. M. Rheima. "Adsorption study of phosphate ions pollution in aqueous solutions using microwave synthesized magnesium oxide nanoparticles." Digest Journal of Nanomaterials and Biostructures 16.3 (2021): 801-807. https://doi.org/10.15251/DJNB.2021.163.801

[17] Abinaya, S., and Helen P. Kavitha. "Magnesium Oxide Nanoparticles: Effective Antilarvicidal and Antibacterial Agents." ACS omega 8.6 (2023): 5225. https://doi.org/10.1021/acsomega.2c01450

[18] Sutapa, I. Wayan, et al. "Synthesis and structural profile analysis of the MgO nanoparticles produced through the sol-gel method followed by annealing process." Oriental Journal of Chemistry 34.2 (2018): 1016. https://doi.org/10.13005/ojc/340252

[19] Mohammed, Gh, Adel M. El Sayed, and W. M. Morsi. "Spectroscopic, thermal, and electrical properties of MgO/polyvinyl pyrrolidone/polyvinyl alcohol nanocomposites." Journal of Physics and Chemistry of Solids 115 (2018): 238-247. https://doi.org/10.1016/j.jpcs.2017.12.050

[20] Rempel, Suzana, et al. "Toxicity effects of magnesium oxide nanoparticles: a brief report." Matéria (Rio de Janeiro) 25 (2020). https://doi.org/10.1590/s1517-707620200004.1170

[21] El-Nahhal, Issa M., et al. "Silica, mesoporous silica and its thiol functionalized silica coated MgO and Mg (OH) 2 materials." Chemistry Africa 2 (2019): 267-276. https://doi.org/10.1007/s42250-019-00063-0

[22] Karthik, K., et al. "Fabrication of MgO nanostructures and its efficient photocatalytic, antibacterial and anticancer performance." Journal of Photochemistry and Photobiology B: Biology 190 (2019): 8-20. https://doi.org/10.1016/j.jphotobiol.2018.11.001

[23] Basha, Mohammad Ahmed-Fouad. "Magnetic and optical studies on polyvinylpyrrolidone thin films doped with rare earth metal salts." Polymer journal 42.9 (2010): 728-734. https://doi.org/10.1038/pj.2010.60

[24] Song, Y. J., Wang, M., Zhang, X. Y., Wu, J. Y., & Zhang, T.. “Investigation on the role of the molecular weight of polyvinyl pyrrolidone in the shape control of high-yield silver nanospheres and nanowires.” Nanoscale research letters, 9(2014): 1-8.

[25] Khan, A., et al. "Mechanistic study on methyl orange and congo red adsorption onto polyvinyl pyrrolidone modified magnesium oxide." International Journal of Environmental Science and Technology (2021): 1-14.

[26] Liu, He, et al. "Hydrothermal synthesis of monodisperse Ag2Se nanoparticles in the presence of PVP and KI and their application as oligonucleotide labels." Journal of Materials Chemistry 18.22 (2008): 2573-2580. https://doi.org/10.1039/b719207j

[27] Pan, Mingming, et al. "Photosensitivity enhancement at visible in Polyvinylpyrrolidone-based polymers doped

with Fe and Cu ions." Chemical Physics Letters 754 (2020): 137640. https://doi.org/10.1016/j.cplett.2020.137640
[28] Vani, G. Naga Sudha, et al. "Optical properties of PVP based polymer electrolyte films." Int. J. Res. Eng. Adv. Technol. 3 (2013): 7-12.
[29] Mohammed, M. I. "Controlling the optical properties and analyzing mechanical, dielectric characteristics of MgO doped (PVA-PVP) blend by altering the doping content for multifunction.
[30] Halder, R., and S. Bandyopadhyay. "Synthesis and optical properties of anion deficient nano MgO." Journal of Alloys and Compounds 693 (2017): 534-542. https://doi.org/10.1016/j.jallcom.2016.09.164
[31] Venugopal, Gunasekaran, et al. "Structural and mechanical properties of MgO-poly (vinyl alcohol) nanocomposite film." Advanced Science, Engineering and Medicine 7.6 (2015): 457-464. https://doi.org/10.1166/asem.2015.1714
[32] Ramadan, Ahmed A., Robert D. Gould, and Ahmed Ashour. "On the Van der Pauw method of resistivity measurements." Thin solid films 239.2 (1994): 272-275. https://doi.org/10.1016/0040-6090(94)90863-X
[33] Oliveira, F. S., et al. "Simple analytical method for determining electrical resistivity and sheet resistance using the van der Pauw procedure." Scientific Reports 10.1 (2020): 16379. https://doi.org/10.1038/s41598-020-72097-1
[34] Krupka, Jerzy. "Contactless methods of conductivity and sheet resistance measurement for semiconductors, conductors and superconductors." Measurement Science and Technology 24.6 (2013): 062001. https://doi.org/10.1088/0957-0233/24/6/062001
[35] Náhlík, Josef, Irena Kašpárková, and Přemysl Fitl. "Study of quantitative influence of sample defects on measurements of resistivity of thin films using van der Pauw method." Measurement 44.10 (2011): 1968-1979.https://doi.org/10.1016/j.measurement.2011.08.02

How to Cite

Z. D. . Abd Ali, A. A. . Ahamed, O. A. A. . Dakhil, and A. . Albeer, “Optical and Electrical Properties of Nano Magnesium Oxide Doped with Polyvinylpyrrolidone (PVP)Thin Films: Conductivity of composite polymer thin films doped with nano metal oxide”, *Al-Mustansiriyah Journal of Science*, vol. 34, no. 4, pp. 129–137, Dec. 2023.